

FOVEATED NONLOCAL DUAL DENOISING

Tao Dai*, Ke Gu†, Qingtao Tang*, Kwok-Wai Hung‡, Yong-bing Zhang*, Weizhi Lu* Shu-Tao Xia*

*Graduate School at Shenzhen, Tsinghua University, Shenzhen, Guangdong, China

†Faculty of Information Technology, Beijing University of Technology, 100124, China

‡College of Computer Science and Software Engineering, Shenzhen University

Email: dait14@mails.tsinghua.edu.cn

ABSTRACT

Recently developed dual domain image denoising (DDID) algorithm and its variants, such as dual domain filter (DDF), achieve remarkable results by combining bilateral filter with frequency-based method. However, this kind of algorithms require large patches to guarantee the denoising performance and most of them produce ringing artifacts due to the Gibbs phenomenon induced by high-contrast details. To address these issues, we propose a Foveated Nonlocal Dual Denoising (FNDD) algorithm by unifying foveated nonlocal means and frequency-based methods. In this way, the ability to preserve the high-contrast details is noticeably improved by exploiting foveated self-similarity (patch similarity) instead of pixel similarity, thus leading to void of artifacts. Moreover, we propose an entropy-based back projection step for compensating the detail loss to further improve the performance. Experimental results validate that FNDD significantly outperforms DDID in terms of both quantitative metrics and subjective visual quality under much smaller patches, and even achieves comparable results against state-of-the-art competitors.

Index Terms— Image denoising, Dual domain denoising, Foveated self-similarity, Back projection

1. INTRODUCTION

Image denoising is an important preprocessing tool for various applications, such as image enhancement [1], image quality assessment [2], and image superresolution [3]. Recently, many denoising algorithms have been proposed [4, 5, 6]. In general, image denoising methods can be categorized into transform domain method, spatial domain method, or hybrid spatial-transform method.

Transform domain methods assume that images can be properly represented by some basis. In the transformed domains, coefficient compression or thresholding methods, such as BayesShrink [7], SUREShrink [8] and BLS-GSM [9], are adopted to suppress the noise component. Although transform domain methods remove noise and preserve edges of images effectively, they also introduce strong ringing artifacts due to the Gibbs phenomenon. The ringing artifacts not only alter the original image structures, but also seriously affect the visual effect. On the contrary, spatial domain

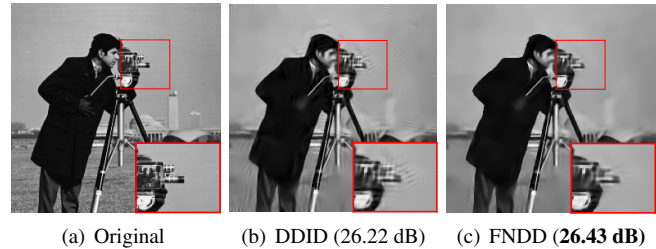


Fig. 1. Panels (a-c) show the original image *Cameraman* (at $\sigma = 50$), the denoised results of DDID and FNDD.

methods can obtain smoother images with much less artifacts. Recently, spatial domain methods achieve remarkable results by exploiting non-local self-similarity, inherent in the natural images. The non-local means algorithm (NLM) [10] and its variants [11, 12] are typical examples of spatial domain methods. The basic idea of these non-local methods relies in averaging similar pixels, measuring their similarity with patches. Since then, more generalized patch-based methods have been developed [13, 14, 15, 16]. Among them, Elad *et al.* [14] propose sparse representations of patches using dictionaries. In a different direction, Lebrun *et al.* propose non-local bayes (NLB) to solve the most likely patches by matrix inversion. Spatially adaptive iterative singular-value thresholding (SAIST) [16] achieves remarkable results by using self-similarity and low rank approximation.

Most state-of-the-art algorithms take advantage of both spatial and transform domain methods [13, 17, 18, 19]. Among them, block matching and 3-D (BM3D) [13] and its variant BM3D-SAPCA [17] combine non-local means and transform domain methods. The main drawback of these patch-based methods is that most of them demand high computational burden and produce annoying artifacts.

Different from the traditional hybrid methods, recently a simple and effective method, dual domain image denoising (DDID) [18], has been proposed by combining bilateral filter and frequency-based method. Besides the simple implementation, DDID provides results that are generally superior to methods such as BM3D or NLB. However, DDID generates typical frequency domain artifacts, especially on sharp edges of the original image, as shown in Fig. 1 (b).

To remove the artifacts produced by other state-of-the-art methods (e.g. BM3D) or avoid the appearance of the artifacts in DDID, some methods, such as PID [20], DDF [21] and NLDD [22] are proposed. Among them, NLDD removes the artifacts in DDID with a high-quality guide image, obtained by NLB. By contrast, PID and DDF are mainly used as post-processing methods to improve the results with more iterations by eliminating the artifacts of state-of-the-art methods (e.g. BM3D). Therefore, their success depends on

This work is supported by the National Natural Science Foundation of China under grant Nos.61371078, 61375054, the R&D Program of Shenzhen under grant Nos.JCYJ20140509172959977, JSGG20150512162853495, ZDSYS20140509172959989, JCYJ20160331184440545, JCYJ20160513013916577, and the Guangdong Special Support program (2015TQ01X161).

the use of the high-quality guide image, the use of large (31×31) patches or with more iterations, but these conditions cannot be always satisfied in practical applications. This observation inspires us to develop a new denoising algorithm. Namely, with the noisy guide image, smaller patches (10×10) and a few iterations, we show in this paper that our method can yield high-quality results by combining foveated NLM [23] and frequency-based method.

Contribution. This paper presents a Foveated Nonlocal Dual Denoising (FNDD) algorithm, which consists of exploiting foveated self-similarity in spatial domain and wavelet shrinkage in frequency domain. Motivated by the fact that spatial domain methods excel at denoising high-contrast signals, while frequency domain methods excel at denoising low-contrast signals, we split the noisy image into high-contrast layer and low-contrast layer as in DDID [18]. Different from DDID, we exploit foveated self-similarity rather than pixel similarity used in DDID in order to well preserve the high-contrast details. In this way, the subsequently obtained low-contrast signals are more stationary, contributing to avoiding artifacts. On the other hand, we propose an entropy-based back projection to further improve the performance.

2. FOVEATED DISTANCE

We consider observations as noisy grayscale images $y : P \rightarrow \mathbb{R}$ that can be formulated as $y(p) = x(p) + n(p)$, $p \in P \subset \mathbb{Z}^2$, where $P \subset \mathbb{Z}^2$ is the image domain (a regular pixel grid), $x : P \rightarrow \mathbb{R}$ is the unknown original image, and $n : P \rightarrow \mathbb{R}$ is additive Gaussian white noise (AWGN), $n(\cdot) \sim \mathcal{N}(0, \sigma^2)$.

Let $U \subset \mathbb{Z}^2$ be a neighborhood centered at the origin. We define the patch centered at a pixel $p \in P$ in the noisy image y as: $\mathbf{y}_p(u) = y(u+p)$, $u \in U$. The conventional windowed distance is computed between two patches \mathbf{y}_p and \mathbf{y}_q

$$d^{\text{WIN}}(p, q) = \|\mathbf{y}_p^{\text{WIN}} - \mathbf{y}_q^{\text{WIN}}\|^2 = \|\mathbf{y}_p \sqrt{\mathbf{K}} - \mathbf{y}_q \sqrt{\mathbf{K}}\|^2, \quad (1)$$

where $\mathbf{y}_p^{\text{WIN}} = \mathbf{y}_p \sqrt{\mathbf{K}}$ is the windowed patch of size $r \times r$; \mathbf{K} is a non-negative windowing kernel defined over U , which adjusts the contribution of each term depending on the position of $u \in U$.

Similarly, the foveated distance can be formulated as

$$d^{\text{FOV}}(p, q) = \|\mathcal{F}[y, p] - \mathcal{F}[y, q]\|^2 = \|\mathbf{y}_p^{\text{FOV}} - \mathbf{y}_q^{\text{FOV}}\|^2, \quad (2)$$

where $\mathbf{y}_p^{\text{FOV}}$ is a foveated patch obtained by foveation operator \mathcal{F} , which takes the form

$$\mathbf{y}_p^{\text{FOV}}(u) = \mathcal{F}[y, p](u) = \sum_{q \in \mathbb{Z}^2} y(q+p) \nu_u(q-u), \quad u \in U \quad (3)$$

where ν_u is a bivariate elliptical Gaussian PSF producing the blur.

Compared with the conventional windowed distance, the foveated distance mimics the insensitivity of the HVS to details at the periphery of the center of attention. Besides, foveated self-similarity [23, 24] outperforms the conventional windowed self-similarity in the filtering task in terms of contrast and sharpness preserving. For this reason, we integrate foveated self-similarity and frequency-based method into our denoising framework to prevent the appearance of ringing artifacts. For more details about foveated self-similarity, please refer to [23, 24].

3. DUAL DOMAIN IMAGE DENOISING

DDID is first proposed by Knaus *et al.* in [18], including three nearly the same iterations. The basic idea of DDID is to split the images

into high-contrast and low-contrast signals, which are processed by the bilateral filter and wavelet shrinkage method, respectively. The final denoised image \hat{y} can thus be the sum of two denoised layers: $\hat{y} = \hat{y}^l + \hat{y}^h$, where \hat{y}^l and \hat{y}^h denote the denoised results of low-contrast signals y^l and high-contrast signals y^h in y .

To filter a pixel centered at p from the noisy image y , the DDID step extracts a large (31×31) pixel patch \mathcal{N}_p centered at p and the corresponding patch from the guide image g .

The extracted patches are processed by the bilateral filter, thus obtaining the denoised high-contrast value $\hat{y}^h(p)$ and $\hat{g}^h(p)$:

$$\hat{y}^h(p) = \frac{\sum_{q \in \mathcal{N}_p} k(q)y(q)}{\sum_{q \in \mathcal{N}_q} k(q)}, \quad \hat{g}^h(p) = \frac{\sum_{q \in \mathcal{N}_p} k(q)g(q)}{\sum_{q \in \mathcal{N}_q} k(q)}, \quad (4)$$

where the weight function k is

$$k(q) = \exp\left(-\frac{|g(q) - g(p)|^2}{\gamma_r \sigma^2}\right) \exp\left(-\frac{\|q - p\|^2}{2\sigma_s^2}\right). \quad (5)$$

The first term in k identifies the pixels with similar structure to the center pixel, while the second term in k eliminates the periodization discontinuities with respect to a discrete Fourier transform (DFT). The parameters σ_s and γ_r respectively controls the decay of the exponential function; σ is the standard deviation of the noise.

After processing the high-contrast signals by the bilateral filter, the next step is obtaining the low-contrast signals by subtracting the bilaterally filtered high-contrast values $\hat{y}^h(p)$ and $\hat{g}^h(p)$. Subsequently, use wavelet shrinkage in the Fourier domain to remove the noise. Then the denoised low-contrast value $\hat{y}^l(p)$ can be obtained by converting the filtered Fourier coefficients into the image domain. Thus the final denoised value centered at p is the sum of the denoised low-contrast and high-contrast values:

$$\hat{y}(p) = \hat{y}^l(p) + \hat{y}^h(p). \quad (6)$$

A complete DDID step consists of the above process repeated for each pixel of the image. Then the DDID algorithm repeats DDID step three times with different parameter values. Each time the denoised result of the previous iteration is applied as a guide, except in the first iteration where the noisy image is used as a guide. For more details about DDID refer to [18, 22].

Although DDID can remove the noise effectively, its denoised results often show strong ringing artifacts especially at the high noise levels. As shown in Fig. 1(b), we can see that many artifacts appear around the edges of the image *Cameraman*. The main reason for this phenomenon is that in the first iteration, the pixel correlations would be seriously corrupted especially at the high noise levels. Then the subsequent frequency domain denoising may contain rich high-contrast details, thus leading to strong artifacts.

Since we know the origins of the artifacts, replacing pixel similarity used in DDID with (foveated) patch similarity is a natural thought. In this way, the high-contrast details can be better preserved, contributing to prevent the appearance of artifacts. Besides introducing artifacts, another drawback of DDID is that it requires large (31×31) patches to guarantee its performance.

To overcome these drawbacks, we propose a Foveated Nonlocal Dual Denoising algorithm by embedding exploiting foveated self-similarity (patch similarity) and frequency-based denoising into an integral denoising framework, which yields remarkable results with much smaller (10×10) patches.

4. FOVEATED NONLOCAL DUAL DENOISING

The proposed FNDD mainly consists of three parts, i.e. foveated NLM, entropy-based back projection and frequency-based denois-

ing steps, as shown in Fig. 2. It can be observed that the first step splits the noisy image into the denoised high-contrast signals and the noisy low-contrast signals by foveated NLM. The second step uses back projection step to recover the lost details, thus yielding a new guide image. The last step filters the noisy low-contrast signals by frequency-based denoising step.

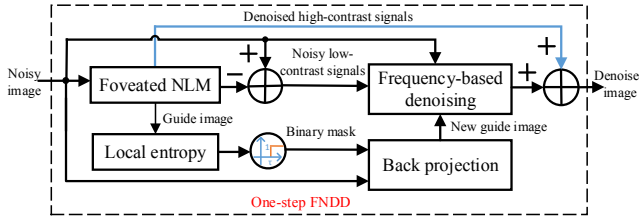


Fig. 2. Flow chart of the proposed FNDD

4.1. Exploit foveated self-similarity in spatial domain

In the first step, we compute the denoised high-contrast value $\hat{y}^h(p)$ and $\hat{g}^h(p)$ from the noisy image y and the guide image g using (4). The main difference between FNDD and the original DDID lies in similarity measure. Further, FNDD adopts (foveated) patch similarity rather than pixel similarity used in DDID, and thus we can obtain a new weight function k' based on patch similarity,

$$k'(q) = \exp\left(-\frac{\|\mathbf{g}_p^{\text{FOV}} - \mathbf{g}_q^{\text{FOV}}\|^2}{\gamma_{rr}\sigma^2}\right) \exp\left(-\frac{\|q - p\|^2}{2\sigma_s^2}\right), \quad (7)$$

where $\mathbf{g}_p^{\text{FOV}}$ and $\mathbf{g}_q^{\text{FOV}}$ are foveated patches of size $r \times r$, belonging to a search window of size $d \times d$; the foveated patches are obtained by foveated operator \mathcal{F} in (3); γ_{rr} and σ_s control the decay of the exponential function, and σ is the standard deviation of the noise.

With the new weight function, the noisy image can be split into high-contrast and low-contrast layers more accurately, in spite of strong noise levels. In implementation, the foveated NLM is used to filter the noisy image, thus producing a cleaner guide image.

4.2. Entropy based back projection

In the second step, we try to recover the lost details from residual image to the guide image. In our method, the guide image plays a critical role in the denoising performance, since it is used to guide the frequency-based denoising. Nevertheless, the guide image g obtained by (7) can be easily over-smoothed due to the characteristic of patch similarity. To further improve the denoising performance, it is necessary to retrieve the lost original structures. To that end, back projection is such an efficient method successfully used in [25]. The basic idea of back projection is to create a new noisy image g' by

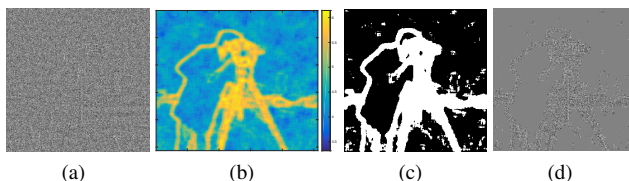


Fig. 3. From left to right: panels (a-d) show (a) residual image, (b) entropy map, (c) binary entropy map (The white stands for 1, while the black stands for 0), and (d) the extracted residual image.

Algorithm 1 Foveated Nonlocal Dual Denoising

```

Input: Noisy image  $y$  with  $\sigma^2$ , patch size  $r$  and search window size  $d$ 
Output: Denoised image  $\hat{y}$ 

1:  $g \leftarrow \text{FoveatedNLM}(y, d, r, \sigma)$  //Filter  $y$  by Eq. 7
2:  $e \leftarrow \text{EntropyCompute}(g)$  //Eq. 8
3:  $g' \leftarrow \text{BackProjection}(g, e)$  //Eq. 9
4: for each pixel  $p$  in  $y$  do
5:    $y_p \leftarrow \text{EXTRACTPATCH}(y, p)$ 
6:    $\mathbf{g}_p \leftarrow \text{EXTRACTPATCH}(g', p)$ 
7:    $\mathbf{g}_p^{\text{FOV}}, \mathbf{g}_q^{\text{FOV}} \leftarrow \mathcal{F}[\mathbf{g}', p]$  // Eq. 3
8:    $k' \leftarrow \text{ComputeK}(\mathbf{g}_p^{\text{FOV}}, \mathbf{g}_q^{\text{FOV}})$  // Eq. 7
9:    $\hat{y}^h(p) \leftarrow \left( \frac{\sum k'(q)y(q)}{\sum k'(q)} \right)$ 
10:   $\hat{g}^h(p) \leftarrow \left( \frac{\sum k'(q)g'(q)}{\sum k'(q)} \right)$ 
11:   $Y \leftarrow \sum \exp\left(\frac{-2i\pi(q-p)f}{d}\right) k'(q) (y(q) - \hat{y}^h(p))$  // DFT
12:   $G \leftarrow \sum \exp\left(\frac{-2i\pi(q-p)f}{d}\right) k'(q) (g'(q) - \hat{g}^h(p))$ 
13:   $\sigma_f^2 \leftarrow \sigma^2 \sum (k'(q))^2$  // Noise level in frequency domain
14:   $K \leftarrow \exp\left(\frac{-\gamma_f \sigma_f^2}{|G(f)|^2}\right)$  // Shrinkage operator
15:   $\hat{y}^l(p) \leftarrow \frac{1}{d^2} \sum_f Y(f) K(f)$  //Inverse DFT transform
16:   $\hat{y}(p) \leftarrow \hat{y}^h(p) + \hat{y}^l(p)$  //The final denoised pixel
17: end for
18:  $\hat{y} \leftarrow \text{Return the denoised image.}$ 

```

adding the residual image ($y - g$) back to the denoised image g , i.e., $g' = g + \delta(y - g)$, where $\delta \in (0, 1)$ is a projection parameter. Nevertheless, this simple idea cannot always improve the performance due to the very low Signal-noise ratio (SNR) of the residual image. To better recover the lost details as well as reduce the effect of noise from residual image, we propose an entropy based back projection step. From the analysis of local entropy [26], we can know that local entropy is relatively small in homogeneous neighborhoods (e.g. background) but relatively large in heterogeneous regions (e.g. area of edges), as shown in Fig. 3 (b). Motivated by this fact, we can obtain the position information corresponding to heterogeneous regions by thresholding entropy values of g . Besides, local entropy of a pixel centered at p is calculated in a neighborhood Ω ,

$$e(p) = \sum_{k \in \Omega} P_k \log P_k, \quad (8)$$

where P_k is the probability of gray level k appearing in the neighborhood centered at p . Then we add the residual image that corresponds to heterogeneous regions back to the guide image g , thus yielding a new guide image g' ,

$$g' = g + (y - g) \cdot \text{BW}(e, \tau), \quad (9)$$

where $\text{BW}(e, \tau) = \begin{cases} 1, & \text{if } e(p) > \tau \\ 0, & \text{otherwise} \end{cases}$ is a binary mask operator with thresholding τ ; the dot \cdot means that multiplication is pixel-wise. Follow the work in [26], we set $\tau = \alpha \max_p e(p)$, $\alpha \in [0.8, 0.9]$.

We illustrate the effect of our entropy based back projection in Fig. 3. It can be observed that most areas in residual image behave more like noise, while the original image structures (e.g. edges) still exist in corresponding heterogeneous regions. From Fig. 3 (d), it can be seen that the extracted residual image contains the structures of the original image (e.g. area of camera bracket).

4.3. Wavelet shrinkage in frequency domain

In the last step, we shrink the noisy Fourier coefficients with shrinkage operator, which is similar to the weight function of the bilateral

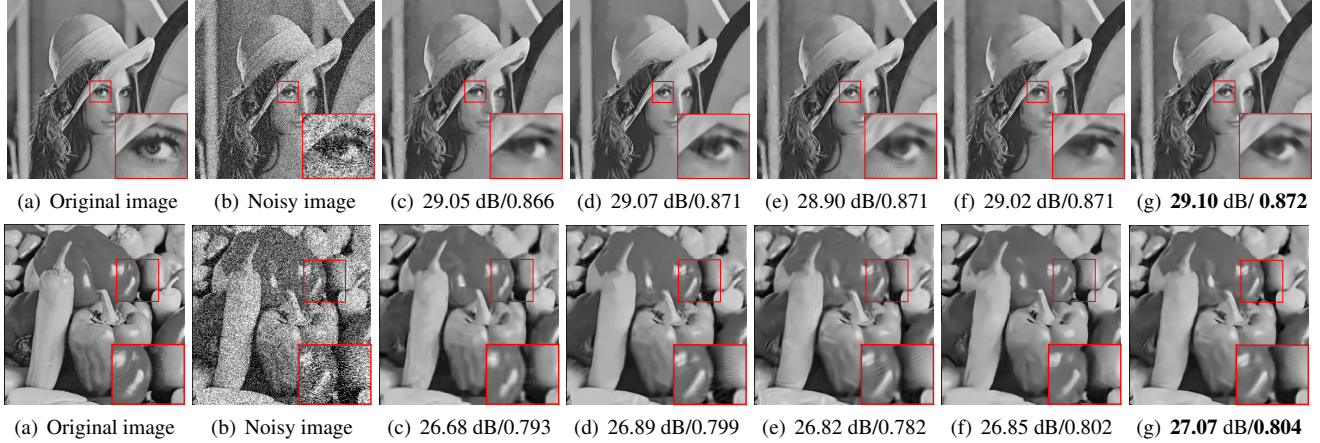


Fig. 4. Denoised results of the images Lena (the first row) and Peppers (the second row) (at $\sigma = 50$) with (c) BM3D, (d) SAIST, (e) DDID, (f) NLDD, and (g) the proposed FNDD. Zoom into PDF file for a detailed view.

filter (see line 14 in Algorithm 1). The wavelet shrinkage procedure consists of DFT transform, shrinkage of the frequency coefficients and inverting the DFT transform (see lines 11-15 in Algorithm 1). By the shrinkage operator, the signal is kept while the noise is discarded. The denoised low-contrast value is obtained by converting the DFT transform to the spatial domain (see line 15 in Algorithm 1). A pseudo-code for FNDD is listed in Algorithm 1.

5. EXPERIMENTAL RESULTS

To test the performance of the proposed FNDD comprehensively, extensive experiments are performed on multiple test images from the standard image database. All the results are evaluated with PSNR and Structural Similarity index (SSIM) [27]. Each image is contaminated with AWGN with different amounts of noise, but we report the typical results ($\sigma = 30, 50$) due to the limited space. At other noise levels, the results are similar to the reported results.

FNDD has been compared against several state-of-the-art algorithms, i.e., BM3D [13], SAIST [16], DDID [18] and NLDD [22]. The parameters of these comparing methods are set as the default values. For FNDD, the parameters $r = 3, d = 10, \sigma_s = 7, \tau = 0.8, \delta = 0.4$ are chosen empirically; we iterate FNDD twice with $\gamma_f = 0.3, 0.5$, and $\gamma_{rr} = 1, 1.5$ for the first and second iteration, respectively; local entropy is computed in 7×7 patches.

PSNR and SSIM results are summarized in Table 1. Compared with other four methods, it can be seen that FNDD obtains the best results in terms of PSNR and SSIM on the images with more smooth regions, such as *Lena* and *Montage*. Moreover, FNDD outperforms DDID in most cases, which mainly benefits from foveated self-similarity. Note that NLDD obtains the best results on some images. This is because NLDD uses the high-quality guide image produced by NLB [15] to guarantee its performance.

We also compare the visual quality in Fig. 4. We can see that the denoised results of NLDD and FNDD are very similar in visual perception, and are clearly better than other methods. For example, noticeable artifacts exist in the denoised images produced by BM3D, SAIST and DDID, but less artifacts can be noticed in the denoised results of NLDD and FNDD. FNDD also works well in preserving local structures (e.g. the eye area of *Lena*).

In addition, FNDD is faster than DDID, as smaller patches are used. The source code of both DDID and FNDD is written

Table 1. PSNR and SSIM of BM3D, SAIST, DDID, NLDD and the proposed FNDD with various tested images for various σ . (From top to bottom is the image *Lena*, *Barbara*, *Boat*, *House*, *Pepper*, *Camerman*, *Montage* and *Man*. The last row is the average results.)

	σ	BM3D	SAIST	DDID	NLDD	FNDD
L.	30	31.26/.911	31.32/.915	31.35/.918	31.27/.914	31.36/.919
	50	29.05/.866	29.07/.871	28.90/.871	29.02/.871	29.10/.872
B.	30	29.81/.927	30.08/.930	29.84/.929	29.78/.931	29.67/.928
	50	27.22/.872	27.52/.877	27.31/.876	27.07/.865	27.11/.873
Bo.	30	29.12/.887	28.92/.872	28.93/.881	28.83/.870	28.90/.879
	50	26.78/.817	26.54/.786	26.55/.801	26.60/.785	26.55/.804
H.	30	32.09/ .849	32.18/.849	31.77/.838	32.18/.847	31.80/.845
	50	29.69/.814	30.09/.822	29.21/.791	29.48/.815	29.45/.809
P.	30	29.28/.852	29.33/.852	29.39/.845	29.62/.860	29.48/.854
	50	26.68/.793	26.89/.799	26.82/.782	26.85/.802	27.07/.804
Ca.	30	28.64/.830	28.30/.823	28.52/.819	28.80/.847	28.53/.831
	50	26.12/.775	26.10/.774	26.22/.760	26.59/.787	26.43/.787
M.	30	31.37/.907	30.95/.917	31.41/.904	31.52/.922	31.76/.923
	50	27.90/.857	27.83/.871	28.23/.846	28.67/.877	28.83/.879
Ma.	30	28.86/.875	28.75/.860	28.73/.866	28.86/.864	28.89/.876
	50	26.81/.804	26.67/.783	26.64/.787	26.81/.789	26.83/.805
Av.	30	30.05/.879	29.97/.877	29.99/.875	30.10/.881	30.04/.881
	50	27.53/.824	27.58/.822	27.48/.814	27.63/.823	27.66/.827

in Matlab, and the platform is on a 2-core 2.6 GHz Intel Core i5. The implementation of DDID and FNDD takes 48 seconds and 32 seconds, respectively, to denoise a 256×256 gray-scale image.

6. CONCLUSIONS

The proposed Foveated Nonlocal Dual Denoising (FNDD) algorithm in this paper consists of three modules: exploiting foveated self-similarity, entropy based back projection, and frequency-based denoising step. Compared with other methods built on DDID, FNDD yields high-quality results with much smaller patches (10×10). Besides, considering the trade-off between computational complexity and the performance, our method iterates twice with empirically selected parameter values. Note that recent work [28] proposes a parameter trimming framework that incorporates the quality monitor into the denoising algorithms for the optimal parameter selection. It can be expected that the performance of our method can be further improved with the optimal parameter values, obtained by the parameter selection [28]. These works will be studied in future works.

7. REFERENCES

- [1] K. Gu, D. Tao, J. F. Qiao, and W. Lin, “Learning a no-reference quality assessment model of enhanced images with big data,” *IEEE Transactions on Neural Networks and Learning Systems*, vol. PP, no. 99, pp. 1–13, 2017.
- [2] H. Liang and D. Weller, “Comparison-based image quality assessment for selecting image restoration parameters,” *IEEE Transactions on Image Processing*, vol. PP, no. 99, pp. 1–1, 2016.
- [3] Ji-Ping Zhang, Tao Dai, and Shu-Tao Xia, “Single-frame super-resolution via compressive sampling on hybrid reconstructions,” in *International Conference on Neural Information Processing*. Springer, 2015, pp. 610–618.
- [4] Shao Ling, Yan Ruomei, Li Xuelong, and Liu Yan, “From heuristic optimization to dictionary learning: A review and comprehensive comparison of image denoising algorithms,” *Cybernetics, IEEE Transactions on*, vol. 44, no. 7, pp. 1001–1013, 2014.
- [5] Tao Dai, Weizhi Lu, Wei Wang, Jilei Wang, and Shu-Tao Xia, “Entropy-based bilateral filtering with a new range kernel,” *Signal Processing*, vol. 137, pp. 223 – 234, 2017.
- [6] Zhiyuan Zha, Xin Liu, Ziheng Zhou, Xiaohua Huang, Jingang Shi, Zhenhong Shang, Lan Tang, Yechao Bai, Qiong Wang, and Xinggan Zhang, “Image denoising via group sparsity residual constraint,” *CoRR*, vol. abs/1609.03302, 2016.
- [7] S Grace Chang, Bin Yu, and Martin Vetterli, “Adaptive wavelet thresholding for image denoising and compression,” *Image Processing, IEEE Transactions on*, vol. 9, no. 9, pp. 1532–1546, 2000.
- [8] Florian Luisier, Thierry Blu, and Michael Unser, “A new sure approach to image denoising: Interscale orthonormal wavelet thresholding,” *Image Processing, IEEE Transactions on*, vol. 16, no. 3, pp. 593–606, 2007.
- [9] Javier Portilla, Vasily Strela, Martin J Wainwright, and Eero P Simoncelli, “Image denoising using scale mixtures of gaussians in the wavelet domain,” *Image Processing, IEEE Transactions on*, vol. 12, no. 11, pp. 1338–1351, 2003.
- [10] Antoni Buades, Bartomeu Coll, and Jean-Michel Morel, “A review of image denoising algorithms, with a new one,” *Multiscale Modeling & Simulation*, vol. 4, no. 2, pp. 490–530, 2005.
- [11] Charles Kervrann and Jérôme Boulanger, “Optimal spatial adaptation for patch-based image denoising,” *Image Processing, IEEE Transactions on*, vol. 15, no. 10, pp. 2866–2878, 2006.
- [12] S.P. Awate and R.T. Whitaker, “Unsupervised, information-theoretic, adaptive image filtering for image restoration,” *Pattern Analysis and Machine Intelligence, IEEE Transactions on*, vol. 28, no. 3, pp. 364–376, March 2006.
- [13] K. Dabov, A. Foi, V. Katkovnik, and K. Egiazarian, “Image denoising by sparse 3-d transform-domain collaborative filtering,” *Image Processing, IEEE Transactions on*, vol. 16, no. 8, pp. 2080–2095, Aug 2007.
- [14] Michael Elad and Michal Aharon, “Image denoising via sparse and redundant representations over learned dictionaries,” *Image Processing, IEEE Transactions on*, vol. 15, no. 12, pp. 3736–3745, Dec 2006.
- [15] M. Lebrun, A. Buades, and J. M. Morel, “A nonlocal bayesian image denoising algorithm,” *SIAM Journal on Imaging Sciences*, vol. 6, no. 3, pp. 1665–1688, 2013.
- [16] Weisheng Dong, Guangming Shi, and Xin Li, “Nonlocal image restoration with bilateral variance estimation: a low-rank approach,” *Image Processing, IEEE Transactions on*, vol. 22, no. 2, pp. 700–711, 2013.
- [17] Kostadin Dabov, Alessandro Foi, Vladimir Katkovnik, and Karen Egiazarian, “Bm3d image denoising with shape-adaptive principal component analysis,” in *SPARS’09-Signal Processing with Adaptive Sparse Structured Representations*, 2009.
- [18] Claude Knaus and Matthias Zwicker, “Dual-domain image denoising.,” in *Image Processing (ICIP), 2013 IEEE International Conference on*. IEEE, 2013, pp. 440–444.
- [19] Tao Dai, Chao-Bing Song, Ji-Ping Zhang, and Shu-Tao Xia, “Pmpa: A patch-based multiscale products algorithm for image denoising,” in *Image Processing (ICIP), 2015 IEEE International Conference on*. IEEE, 2015, pp. 4406–4410.
- [20] Claude Knaus and Matthias Zwicker, “Progressive image denoising,” *Image Processing, IEEE Transactions on*, vol. 23, no. 7, pp. 3114–3125, 2014.
- [21] C Knaus and M Zwicker, “Dual-domain filtering,” *SIAM Journal on Imaging Sciences*, vol. 8, no. 3, pp. 1396–1420, 2015.
- [22] N. Pierazzo, M. Lebrun, M.E. Rais, J.M. Morel, and G. Facciolo, “Non-local dual image denoising,” in *Image Processing (ICIP), 2014 IEEE International Conference on*. IEEE, Oct 2014, pp. 813–817.
- [23] Alessandro Foi and Giacomo Boracchi, “Foveated self-similarity in nonlocal image filtering,” in *IS&T/SPIE Electronic Imaging*. International Society for Optics and Photonics, 2012, pp. 829110–829110.
- [24] Alessandro Foi and Giacomo Boracchi, “Foveated nonlocal self-similarity,” *International Journal of Computer Vision*, pp. 1–33, 2016.
- [25] Qiang Guo, Caiming Zhang, Yunfeng Zhang, and Hui Liu, “An efficient svd-based method for image denoising,” *IEEE transactions on Circuits and Systems for Video Technology*, vol. 26, no. 5, pp. 868–880, 2016.
- [26] Chengxin Yan, Nong Sang, and Tianxu Zhang, “Local entropy-based transition region extraction and thresholding,” *Pattern Recognition Letters*, vol. 24, no. 16, pp. 2935–2941, 2003.
- [27] Zhou Wang, Alan Conrad Bovik, Hamid Rahim Sheikh, and Eero P Simoncelli, “Image quality assessment: from error visibility to structural similarity,” *Image Processing, IEEE Transactions on*, vol. 13, no. 4, pp. 600–612, 2004.
- [28] Haoyi Liang and Daniel S Weller, “Denoising method selection by comparison-based image quality assessment,” in *2016 IEEE International Conference on Image Processing (ICIP)*. IEEE, 2016, pp. 3106–3110.